RESEARCH ARTICLE | SEPTEMBER 21 2021

Erosion of focus rings in capacitively coupled plasma etching reactors

Xifeng Wang ; Hyunjae Lee; Sang Ki Nam; Mark J. Kushner

Journal of Vacuum Science & Technology A 39, 063002 (2021)
https://doi.org/10.1116/6.0001225

JVST A
Journal of Vacuum Science & Technology A

ARTICLE

avs.scitation.org/journal/jva

Erosion of focus rings in capacitively coupled plasma etching reactors

Cite as: J. Vac. Sci. Technol. A 39, 063002 (2021); doi: 10.1116/6.0001225
Submitted: 19 June 2021 · Accepted: 16 August 2021 ·
Published Online: 21 September 2021

Xifeng Wang,[1,a)] Hyunjae Lee,[2,b)] Sang Ki Nam,[2,c)] and Mark J. Kushner[1,d)]

AFFILIATIONS

[1]Department of Electrical Engineering and Computer Science, University of Michigan, 1301 Beal Ave., Ann Arbor, Michigan 48109-2122
[2]Samsung Electronics Co., Ltd., 129 Samsung-ro, Yeongtong-gu, Suwon-si, Gyeonggi-do 443-742, Republic of Korea

[a)]**Electronic mail:** xifeng.wang@lamresearch.com
[b)]**Electronic mail:** hj0928.lee@samsung.com
[c)]**Electronic mail:** sangki.j.nam@samsung.com
[d)]**Author to whom correspondence should be addressed:** mjkush@umich.edu

ABSTRACT

In plasma etching reactors, the structure surrounding the wafer, often called a focus ring (FR), plays an important role in maintaining uniform fluxes of reactants across the wafer. The FR is typically made of dielectric materials. During the plasma etching process, the sheath that forms over the wafer to accelerate ions anisotropically into the surface extends over the FR. Electrical charging of the FR modifies the sheath relative to that over the wafer. On the one hand, one wants the sheath to be uniform across the wafer-FR boundary to enable uniform fluxes to the edge of the wafer. On the other hand, maintaining a high voltage sheath over the FR will erode the FR, which is undesirable as the FR is a consumable component that must be periodically replaced in high volume manufacturing. In this work, we computationally investigated the consequences of dielectric constant ε_r of the FR materials on erosion of the FR. The series capacitance of the FR and its underlying structure is typically smaller than that of the wafer and its underlying structure. As a result, the FR charges quickly relative to the wafer, which then reduces the voltage across the sheath on top of the FR. The ion energy and angular distributions (IEADs) striking the FR are, therefore, generally lower in energy with a broader angular distribution. With $\varepsilon_r = 2$, the ion energies striking the middle to the outer edge of the FR are 30–180 eV, whereas for $\varepsilon_r = 100$, the ion energies are 120–380 eV. At the transition between the wafer and the FR, there is a skew in the IEAD as large as 15° that results from the difference in sheath thickness above the wafer and the FR. This skew and the erosion rate across the FR are functions of the dielectric constant of the FR material. With low ε_r, the FR charges quickly, less plasma is produced above the FR, and there is less voltage across the sheath that results in less FR erosion. Increasing ε_r of the FR produces a higher sheath voltage as well as higher ion fluxes over the FR, which increases erosion, while the skew at the edge of the wafer is less severe. The material of the subsurface portion of the FR, which dominates its capacitance, is an important consideration in the design of the substrate assembly.

I. INTRODUCTION

Uniformity of reactant fluxes to the wafer during plasma etching and deposition for microelectronics fabrication is a demanding requirement.[1] Edge-exclusion refers to that portion of the wafer at the outer radius that does not produce useful devices due to there being nonoptimum fluxes of radicals and ions, or perturbations in the ion energy and angular distribution (IEAD).[1] Minimizing edge-exclusion requires a smooth transition in reactant fluxes from the edge of the wafer to the supporting structure—the substrate or chuck—surrounding the wafer. To produce this smooth transition, the chemical and electrical properties of the materials surrounding the wafer should also have a smooth transition. This is challenging due to electric field enhancement that occurs at sharp edges and material transitions, and differences in surface reaction rate coefficients.[2,3] A focus ring (FR) typically surrounds the wafer and powered substrate with the goal of providing this smooth transition in reactant fluxes to the edge of the wafer and so minimize edge-exclusion.[4]

An FR usually consists of stacks of dielectric annuli engineered to provide these smooth transitions.[2–10] In order to facilitate placement and removal of the wafer, there is a mechanical gap between the wafer and FR that should be kept as small as possible to prevent perturbations in electric fields and gas flow, and to prevent unwanted deposition in the wafer-FR gap.[11,12]

In radio frequency (RF) capacitively coupled plasma (CCP) reactors, power is coupled into the plasma by an oscillating sheath formed over the wafer. Power consists of electron heating and acceleration of ions onto the surface of the wafer. The capacitive power dissipation extends beyond the limits of the wafer due to displacement current that flows through the FR. The end result is that a sheath is formed and power is dissipated at the surface of the focus ring. The sheath is conformal to the surface if the sheath thickness is smaller than characteristic dimensions. This is particularly relevant to plasma penetration into the wafer-FR gap. Denpoh and Shirafuji[12] and Babaeva and Kushner[11] numerically investigated the conformal nature of the sheath around the wafer, focus ring, and wafer-FR gap. They found that plasma penetration and acceleration of ions into the wafer-FR increase as the gap size approaches and exceeds the Debye length. Babaeva and Kushner[13] also found that IEADs striking surfaces in the gap are sensitive to the dielectric constant and height of FR. Kim *et al.*[10] numerically investigated the consequences of the wafer-FR gap size and height and permittivity of the FR in a CCP at a pressure of a few Torr as used for deposition. They found that more uniform fluxes at the edge of wafer can be achieved with a smaller gap and higher FR and that the magnitude of ion fluxes onto the FR is sensitive to the dielectric constant of the FR.

Kim and Economou[2] numerically investigated the sheath properties of and ion fluxes at the transition between a conductor and insulator on the powered electrode of a CCP as an analog to an FR. They found that the sheath potential and sheath thickness at the surface of the focus ring were functions of its height, a consequence of the change in capacitance of the FR. A thicker FR produced a smaller capacitance, which resulted in a smaller sheath thickness.

In most plasma etching tools used in high volume manufacturing (HVM), the FR is a consumable component. That is, there is expected to be plasma erosion of the FR. When the FR erodes to the degree that the tool falls out of specifications, the FR is replaced during scheduled maintenance of the reactor. As a result, there is great motivation to minimize the erosion of the FR to both maintain the desired specifications of the process and to minimize the cost and frequency of replacing the FR. The erosion of the FR is a function of the material of the FR, the magnitude of the ion fluxes incident onto the FR, and the IEADs of those ions.

In this work, we report on a computational investigation of the consequences of FR capacitance on the IEADs incident onto the edge of the wafer and FR in a dual-frequency CCP. When plasma etching high aspect ratio (HAR) features, IEADs with high energy and narrow angular distributions are desired while also controlling the magnitude of the ion fluxes. In dual-frequency CCPs, the high frequency (HF) (more efficient at heating electrons and producing ionization) bias is used to control the magnitude of the ion flux. The low frequency (LF) bias on the substrate is used to control the properties of the IEADs. A feature profile model was used to assess the erosion rate of the FR. We found that the IEADs incident onto the FR are sensitive functions of the dielectric constant of the FR. Low values of dielectric constant result in rapid charging of the FR, which then reduces the sheath voltage on top of the FR, thereby reducing ion energies onto the FR. This, in turn, reduces the erosion rate of the FR. However, these conditions also produce the largest difference in sheath potentials and thickness across the edge of the wafer. This difference in sheath potential can result in angular skewing of the IEAD. Large values of dielectric constant of the FR produces a more uniform sheath structure across the edge of the wafer but also increases the sheath voltage over the FR. The end result is more erosion of the FR. The consequences of power of the low frequency substrate bias on FR erosion were also investigated. In all cases, FR erosion increased with bias power. However, low values of dielectric constant were less sensitive to bias power due to the consistently lower sheath potential at the surface of the FR. The material of the subsurface portion of the FR, which dominates its capacitance, is an important consideration in design of the substrate assembly. Given that the subsurface material can be isolated from the plasma by barrier coatings, there is wide range in the choice of the subsurface material.

The models used in this investigation are briefly described in Sec. II. The ion fluxes and IEADs onto the wafer and FR for the base case are discussed Sec. III. Similar trends while varying the dielectric constant of the FR and low frequency bias are discussed in Secs. IV and V. Concluding remarks are in Sec. VI.

II. DESCRIPTION OF THE MODELS

Reactor scale modeling was performed with the Hybrid Plasma Equipment Model (HPEM).[14] The HPEM is a kinetic-fluid hydrodynamics simulation, which combines separate modules that address different physical phenomena in an iterative manner. In this investigation, the major modules used are the Electron Energy Transport Module (EETM), the Fluid Kinetics Poisson Module (FKPM), the Surface Kinetics Module (SKM), and the Monte Carlo Plasma Chemistry Module (MCPCM). The densities of all charged and neutral species and the electrostatic potentials are obtained from the FKPM. Continuity, momentum, and energy equations for all species are solved coincident with Poisson's equation for the electric potential. Charge densities on the surfaces of the dielectrics are computed from the fluxes of electrons and ions from the bulk plasma and secondary electrons leaving the surfaces and coming from other locations collected by those surfaces. The electron energy equation is implicitly integrated in time to provide the electron temperature, impact rate coefficients, and transport coefficients. These coefficients as a function of average electron energy are provided by solutions of Boltzmann's equation for the electron energy distribution. The trajectories of secondary electrons are advanced using Monte Carlo techniques in the EETM, which provides electron impact sources and injected electron charge sources. The compositions of surfaces in contact with the plasma are provided by the SKM. IEADs to the wafer and FR are computed using Monte Carlo techniques in the MCPCM. The gas phase and surface kinetics reaction mechanisms for the $Ar/C_4F_8/O_2$ plasmas discussed here are essentially the same as in Refs. 15 and 16.

Etch rates (ERs) for the SiO_2 covered wafer and FR were predicted using the Monte Carlo Feature Profile Model (MCFPM). The algorithms used in the MCFPM and the etch mechanism for

SiO_2 in fluorocarbon plasmas are described in detail in Ref. 17. Briefly, the MCFPM resolves the material being etched using a three-dimensional mesh having cubic voxels. A material identity is assigned to each voxel. Fluxes of radicals and ions and their energy and angular distributions (EADs) are obtained from the HPEM. Pseudoparticles representing the incident gas-phase species are statistically selected from the fluxes and EADs and directed toward the surface. Upon striking the surface, a reaction is chosen from the reaction mechanism based on the gas-phase-surface material pairing, and the energy and angle of the incident gas-phase species. Statistical techniques are used to select from the possible reactions. Based on the selected reactions, the voxel at the site of incidence is removed (e.g., etch or sputter), material identity is changed (e.g., passivation), new voxel added is to the material (deposition), or the voxel remains unchanged (nonreactive reflection of gas-phase species). Based on these outcomes, the incident gas-phase pseudoparticle is reflected, implanted or deposited. Upon sputtering or chemical etching, a new gas-phase pseudoparticle is launched from the site of the reaction.

The SiO_2 etch mechanism in fluorocarbon plasmas is discussed in Ref. 17 and is briefly summarized here. The SiO_2 can be directly sputtered by ions by

$$SiO_2(s) + I^+ \rightarrow SiO_2 + I(h), \tag{1}$$

where (s) denotes a surface site, I^+ denotes any ion, and I(h) denotes the hot neutral that results from the ion neutralizing on the surface and reflecting. With the exception of neutralization, the reactions for I^+ and I(h) are the same. In the following discussion, *ion* refers to both energetic ions and their hot atom counterpart. $SiO_2(s)$ is chemically sputtered by first being passivated by C_xF_y to form a surface complex,

$$SiO_2(s) + C_xF_y \rightarrow SiO_2C_xF_y(s). \tag{2}$$

The complex is chemically removed by ion bombardment,

$$SiO_2CF_x(s) + I^+ \rightarrow SiF_x + CO_2 + I(h), \quad x = 1\text{–}3, \tag{3a}$$

$$SiO_2C_2F_3(s) + I^+ \rightarrow SiOCF_3(s) + CO + I(h), \tag{3b}$$

$$SiOCF_3(s) + I^+ \rightarrow SiF_3 + CO + I(h). \tag{3c}$$

Low energy ions can also activate $SiO_2(s)$ to form $SiO_2^*(s)$ with a higher reaction probability with incident C_xF_y. Deposition of C_xF_y on top of the $SiO_2C_xF_y(s)$ complex forms a polymer layer of up to a few nanometers in thickness. The polymer is removed through chemical and physical sputtering. An etch stop occurs if the polymer thickness exceeds a critical value above which ions are not able to penetrate to the $SiO_2C_xF_y(s)$ to stimulate etching.

For etching reactions having an energy dependence (e.g., physical sputtering and chemically enhanced etching), the reaction yield for a particle incident onto a surface with an incident energy of E_i and an incident angle of θ with respect to the local surface normal is determined by

$$p(E_i, \theta) = p_0 \left(\frac{E_i - E_{th}}{E_r - E_{th}} \right)^n f(\theta), \tag{4}$$

where E_{th} is the threshold energy, E_r is a reference energy, p_0 is the yield at the reference energy, n is the energy dependent exponent (typically 0.5–1), and $f(\theta)$ is the relative probability at angle of incidence θ.

In the voxel-based MCFPM, the weighting (number of atoms or molecules) of the gas-phase pseudoparticles is the same as that in the material voxels. Although there are algorithms that enable the gas-phase pseudoparticles to have weightings less than the materials voxels, the usual method of simulation is to have the one-to-one correspondence in weightings. In this way, for example, one gas-phase pseudoparticle can passivate a single material voxel. When the reaction yield [Eq. (4)] exceeds unity, additional voxels should be removed to account for the higher rate of material removal. An improved algorithm was implemented in MCFPM to account for $p(E_i, \theta) > 1$. This improved algorithm is described here.

In physical sputtering of a uniform material, a yield greater than unity results from transfer of the incident particle energy to neighboring surface or subsurface sites. The amount of energy transferred to the neighboring sites exceeds the threshold energy for physically sputtering the neighbor. In a heterogeneous material, the neighboring site may not be the same material species as where the incident gas-phase species hit the surface. For example, in plasma etching of Si in chlorine containing gas mixtures, the silicon surface is passivated to form SiCl(s), $SiCl_2(s)$, and $SiCl_3(s)$. The chemical sputtering threshold for $SiCl_3(s)$ is less than that for $SiCl_2(s)$, which is less than that for SiCl(s) which, finally, is less than that for physical sputtering of Si(s). So if a particle striking Si(s) site has $p(E_i, \theta) > 1$ for physical sputtering and its neighbor is $SiCl_n(s)$, which has a lower threshold, then the excess yield would likely chemically sputter the neighboring $SiCl_n(s)$ in the same manner as physically sputtering Si(s).

Recognizing this hierarchy of (chemical) sputtering reactions, equivalent cosputtered surfaces species are defined. An equivalent cosputtered surface species to surface species A(s) are those surface species whose yield for a given incident gas-phase particle is equal to or greater than that for A(s). For example, SiCl(s), $SiCl_2(s)$, and $SiCl_3(s)$ are equivalent cosputtered species to Si(s). $SiCl_2(s)$ and $SiCl_3(s)$ are equivalent cosputtered species to SiCl(s). $SiO_2C_xF_y(s)$ is an equivalent cosputtered species to $SiO_2(s)$. By default, a surface species is equivalent to itself in terms of cosputtering neighbors.

Implementation of the cosputtered algorithm is as follows. When a gas-phase species strikes the surface, a reaction is randomly chosen for a gas-phase species-material voxel pair in the manner described above. If that reaction is a chemical or physical sputtering reaction with $p(E_i, \theta) > 1$, then there is the possibility that more than one voxel would be removed. The excess yield is $\Delta p = p(E_i, \theta) - 1$. A minimum number of additional voxels are removed equal to $Int(\Delta p)$, where Int is the integer function. The remaining yield is then $\Delta p' = \Delta p - Int(\Delta p)$. A random number is then chosen between 0 and 1, $r = [0, 1]$. If $r \leq \Delta p'$, then another voxel is removed, resulting in the total number of voxels removed

being $N_r = 1 + Int(\Delta p) + n'$, where $n' = 0$ or 1 depending on the outcome of the test involving $\Delta p'$.

The voxel at the site of incidence is first removed with creation of gas-phase pseudoparticles representing the etch product. If $N_r > 1$, a search is made of the 26 voxels surrounding the site of incidence to identify equivalent surface species. The search is performed in a random fashion. That is, the order that the neighbors are inspected is a different sequence for each search. If the search finds an equivalent surface species, then that voxel is removed. Additional gas-phase pseudoparticles are created representing the etch products for the removed voxel. The random search is continued until a total of N_r voxels are removed.

The consequences of the cosputtering algorithms are highly condition dependent. For example, for blanket SiO_2 etching of flat surfaces with high ion energies arriving at near normal angle, predicted etch rates could be 50% higher with than without cosputtering. The same is true for low aspect ratio features. In high aspect ratio features, the ion angle of incidence is grazing to the sidewalls, which reduces their yield, which reduces the influence of cosputtering. After several grazing incidence reflections, the ion energy is typically reduced to values where the yields are less than unity, and cosputtering does not have a large effect.

III. ION FLUXES ONTO AND EROSION OF THE FR

A schematic of the dual-frequency CCP reactor used in this investigation is shown in Fig. 1. A 60 MHz HF power source was applied to the top electrode and a 5 MHz LF bias was applied to the bottom electrode. The HF and LF power supplies were connected to the top electrode and substrate through separate blocking capacitors that produced separated DC biases on the top and bottom electrodes. The power of HF and LF for the base case were 600 and 1000 W, values that were obtained by adjusting the applied voltage amplitudes. Quartz surrounded the top electrode and the metal boundaries of the reactor were grounded. The top electrode also served as a gas nozzle, injecting a mixture of $Ar/C_4F_8/O_2 = 75/20/5$ at a flow rate of 600 SCCM. The pressure was maintained at 30 mTorr at the location of a sensor near the pump by adjusting the gas outlet flow rate.

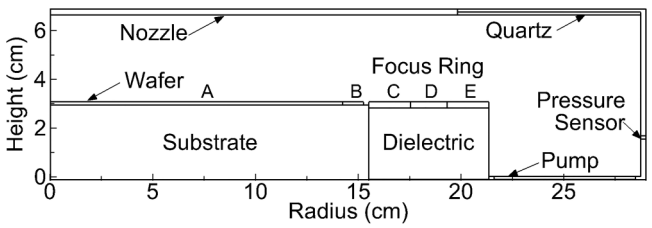

FIG. 1. Schematic of the reactor used in this investigation. The reactor is a dual-frequency capacitively coupled plasma with 60 MHz applied to the top electrode and 5 MHz applied to the bottom electrode. The reactor walls are grounded. Plasma properties and etch rates will be discussed at locations A (center of the wafer), B (edge of wafer), and three locations on the focus ring: C (left edge of FR), D (center of FR), and E (right edge of FR).

The FR surrounding the wafer has a width of 5.85 cm. The top layer of the FR, 0.27 cm thick, was SiO_2 with a dielectric constant of $\varepsilon_r = \varepsilon/\varepsilon_0 = 4.0$. The material underlying the FR was dielectric with $\varepsilon_r = 4$ for the base case. The material of the top surface of the FR is typically chosen for both its electrical and chemical properties. The material for the top of FR should be chemically compatible with the intended process for the wafer. With this goal in mind, the top surface of the focus ring is SiO_2. The permittivity (dielectric constant) of the nonconducting material under the FR can be chosen to control total capacitance of the FR without interfering with the chemical compatibility. The dielectric constant of the underlying material was varied as part of this investigation. Several locations are noted in Fig. 1 where IEADs will be collected and etch rates computed: (A) the center of wafer, (B) edge of wafer, (C) left side of FR, (D) center of wafer, and (E) right side of FR. The IEADs discussed below are averaged over the radial extent of the wafer or FR associated with each site.

Fluxes of neutral radicals and ions to the wafer and FR are shown in Fig. 2. Fluxes of neutrals are fairly uniformly distributed over the surface of both the wafer and FR, with the C_2F_4 flux having the highest value of 3×10^{17} cm^{-2} s^{-1}. In spite of the electron impact sources of these radicals being dominantly over the wafer, their isotropic diffusion extends the fluxes of neutrals to the FR. The magnitudes of ion fluxes are about 2 orders of magnitude smaller than the neutral radicals. The ion fluxes are fairly uniform over the wafer, dominated by Ar^+ with a value of 2×10^{15} cm^{-2} s^{-1}. The fluxes of $C_2F_4^+$ and $C_3F_5^+$ are $0.8–1 \times 10^{15}$ cm^{-2} s^{-1}. Upon transitioning from the wafer to the FR, the ion fluxes decrease by about a factor of about 3. As with the neutral radicals, the electron impact sources for ions are primarily over the wafer. With both the applied and ambipolar electric fields dominantly in the axial direction, the fluxes of ions are also dominantly axial into the wafer. The drift of ions in the radial ambipolar electric fields and radial diffusive flux of ions are smaller in comparison to the axial flux.

The IEADs for all ions are shown in Fig. 3 at locations A and B (wafer center and edge) and across the FR at C (inner edge), D (middle), and E (outer edge). In Fig. 3 and all images of IEADs, a positive angle of incidence indicates an ion slanted toward the center of the wafer. The applied voltage amplitude of the 5 MHz power to deliver 1000 W is 1630 V with a DC bias of −1220 V. The applied voltage amplitude of the 60 MHz power to deliver 600 W is 186 V with a DC bias of −48 V. At the center of the wafer (A), the ion energies extend to 1800 eV with a mean energy of about 1200 eV. The angular spread of the ion flux (FWHM) is ±0.5° and is ±2.1° at 0.1 of the maximum. (Note that the IEADs in all figures are plotted on a two-decade log scale that emphasizes ions arriving at broad angles.) The IEAD at the edge of the wafer (B) has nearly the same dependence in energy as the center. (The less good statistics for the IEAD at B results from the smaller collection area for pseudoparticles at the edge of the wafer.) The IEAD at A is essentially symmetric in angle. The IEAD at B (wafer edge) has an angular skew of about 1.5° at high energies. In transitioning onto the FR (C), the IEAD is significantly skewed in angle, having its centroid at 18°, with a maximum energy of 1500 eV and mean energy of 400 eV. At the center of the FR (D), the IEAD has a maximum energy of 250 eV and mean energy of about 75 eV. The IEAD has a smaller skew of 5°–6° at low energy and a skew of 16°

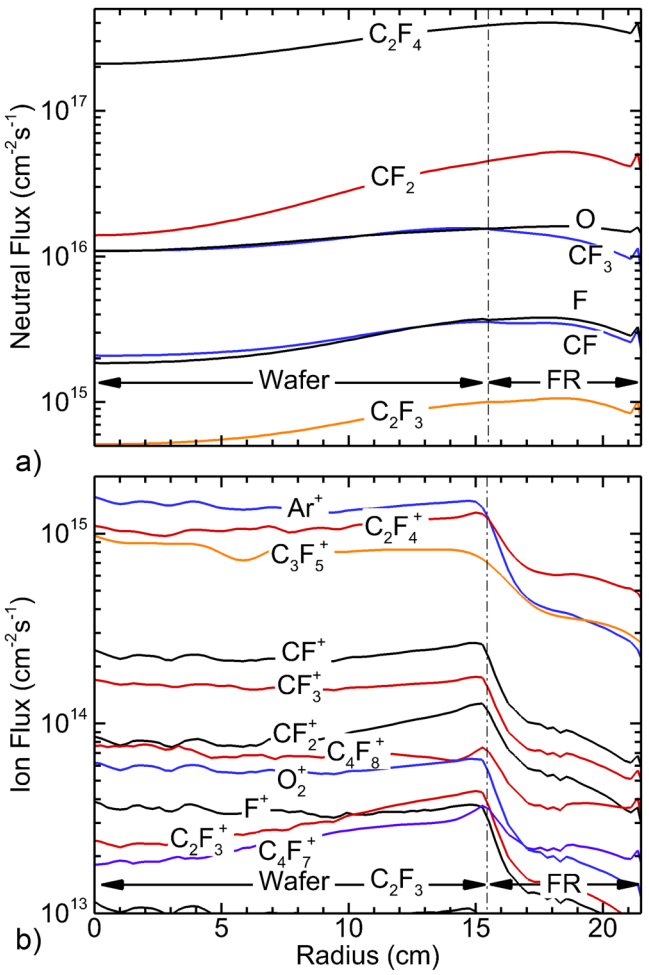

FIG. 2. Time averaged fluxes of (a) radicals and (b) ions to the wafer and focus ring for the base case conditions ($Ar/C_4F_8/O_2$ = 75/20/5, 600 SCCM, 30 mTorr, 60/5 MHz = 600/1000 W. ε_r = 4 for FR). Ion fluxes significantly decrease over the FR relative to the wafer while the neutral fluxes are continuous from the wafer to the FR.

at high energy. At the right edge of the FR (E), the IEAD regains is angular symmetry, though with a maximum energy of only 45 eV and mean energy of 30 eV.

These trends in IEADs are in part explained by the time averaged electron density shown in Fig. 4 for the FR dielectric constant $\varepsilon_r = 4$. The maximum electron density in the bulk plasma is 1.5×10^{10} cm^{-3}. The time averaged edge of the lower sheath is indicated by the 1.5×10^{8} cm^{-3} electron density contour. The time averaged voltage across the sheath is, in part, determined by the sheath's contribution to the series impedance between the powered electrode and ground. The components of this series impedance above the powered electrode include the wafer, sheath, and bulk plasma. The components of this series impedance from the edge of the powered electrode consist of the dielectric materials of the bulk and top of the FR, sheath, and bulk plasma. Above the wafer, the impedance of the sheath is smaller than that of the wafer and bulk plasma. As a consequence, the majority of the applied voltage is dissipated across the sheath, and the maximum energy of the IEAD extends to V_{RF}-V_{DC}. With the sheath boundary being essentially parallel to the wafer extending to nearly the edge of the wafer, the IEAD at A is symmetric in angle.

Over the FR, the largest impedance (smallest capacitance) is that of the FR itself. The RC time constant is sufficiently small that the capacitance of the FR charges to a large fraction of the applied voltage during a single period. This voltage in large part comes at the expense of the sheath voltage. The reduction in sheath potential produces a commensurate thinning of the sheath above the FR. At location C (edge of the FR), the sheath edge is slanted at an angle due to the transition from the thick sheath over the wafer to the thin sheath above the FR. The slant of the sheath edge extends to the edge of the wafer (location B), which produces the small skew in angle at that location. Since the slant in the sheath is largest when the sheath voltage and thickness above the wafer are the largest, the skew in the IEAD at the edge of the wafer is largest at the highest ion energies.

The slant in the sheath transitioning from the wafer to the FR results in the skew in the IEAD at location C. The decrease in the sheath thickness is a consequence of the smaller sheath potential over the FR due to loss of voltage to the charging of the FR capacitance. The smaller sheath potential then produces lower energy ions onto the FR. The transition in the sheath thickness extends to the middle of the FR (location D), providing the skew in the IEAD at that location, though less severe than at the edge of the FR. Here, the skew is more severe at high energy due to the slant in the sheath being greatest at the largest sheath voltage. The sheath thickness is nearly constant and parallel to the surface over the outer edge of the FR (location E), which then restores angular symmetry to the IEAD.

The effective capacitance of the FR at locations C, D, and E are determined by the electric field streamline from the edge of the electrode to the surface of the FR (see Fig. 5). The displacement current through the FR follows this electric field streamline. The capacitance at the surface of the FR is then inversely proportional to the path length along the electric field streamline terminating at the surface. With the electric field streamline from the electrode to the FR at location E being longer than at location C, the capacitance of the FR at its outer edge is smaller, and impedance larger, than at its inner edge. A larger fraction of the applied voltage is, therefore, dissipated in charging the FR at the outer edge of the FR than the inner edge. This produces a thinner sheath, smaller voltage drop across the sheath, and an IEAD with a lower energy at the outer edge of the FR.

On a cycle-averaged basis, there is a dc bias on the substrate. This voltage is dropped between the substrate and, for example, the grounded wall of the chamber. A voltage gradient is then produced across the surface of FR, largely in the radial direction, which is sensitive to the charging of the FR, which is a function of ε_r. The voltage gradient is largely confined to the inner 1/3 of the FR for low ε_r and extends to the outer 1/3 of the FR for large ε_r. This change in voltage gradient then contributes to the skew in the angular distribution of the ions.

The total ion flux to the surface of the wafer and FR and predictions for etch rates for blanket SiO_2 at different locations of the wafer and FR are shown in Fig. 6 for the base case ($\varepsilon_r = 4$) and

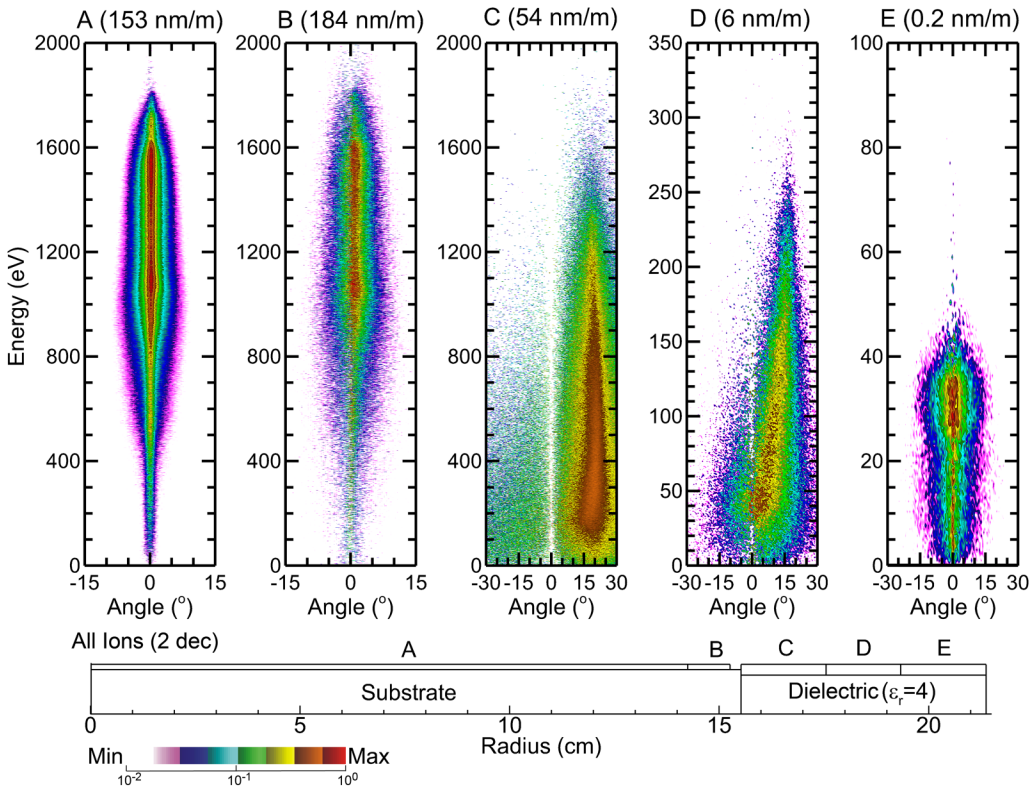

FIG. 3. RF cycle-averaged IEADs of all ions at locations A, B, C, D, and E (noted in the schematic) for the base case conditions ($Ar/C_4F_8/O_2$ = 75/20/5, 600 SCCM, 30 mTorr, 60/5 MHz = 600/1000 W, ε_r = 4 for FR). Each IEAD is separately normalized and plotted on a two-decade log scale.

dielectric constants of the FR material of ε_r = 2–100. For the base case, etch rates over the wafer are 185 nm/m at the (A) center and 195 nm/m at the (B) edge. These predicted etch rates are commensurate with experimental measurements in dual-frequency CCPs for comparable operating conditions.[18,19] The edge-high etch rate results from ion fluxes having a small local maximum at the edge of the wafer due to electric field enhancement at the intersection of the substrate and FR. This electric field enhancement results from the triple point between the plasma, metal electrode, and dielectric. With the radical fluxes nearly constant across the wafer and FR, the decrease in etch rate at the (C) inner edge of the focus ring to 50 nm/m is due to the decrease in ion energy and ion flux. Since the ion energies are still largely above the threshold for chemical sputtering (35 eV), the majority of this decrease is due to the decrease in ion flux. In transitioning across the FR to the (D) middle and (E) outer edge, the etch decreases to near zero as the ion energies decrease below the threshold for chemical sputtering.

IV. CONSEQUENCES DIELECTRIC CONSTANT ON FR EROSION

The dielectric constant of the FR is an important design parameter in determining the electrical properties of the FR. As discussed above, displacement current flows through the FR along the electric field streamlines originating on the biased (metal) electrode and terminating at the surface of the FR. The capacitance along these electric field streamlines decreases with increasing length from the electrode to the surface of the FR, which results in the effective capacitance of the FR being larger at the inner edge (C) and smaller at the outer edge (E). These electric field streamlines are shown in Fig. 5 for ε_r = 2, 20, and 100 averaged over the low frequency RF cycle. The electric field streamlines originate at the top of the FR and terminate on the powered substrate. The difference in capacitance between the inner and outer edge of the FR is greatest for small permittivity due to there being more charging of the top surface.

The permittivity (dielectric constant) of the nonconducting material under the FR was varied to control total capacitance of the FR. SiO_2 remains as the top layer of the FR to maintain the desired chemical compatibility. The electron densities at the edge of the wafer and above the FR for dielectric constants of the focus ring of ε_r = 2, 4, 10, 20, 60, and 100 are shown in Fig. 4. The combined capacitance of the top and subsurface portions of the FR vary from 5.8 pF/cm^2 for ε_r = 2 to 94 pF/cm^2 for ε_r = 100. The total ion fluxes to the wafer and surface of the FR are shown in Fig. 6(a) for the same conditions. The electron densities in the bulk plasma above the

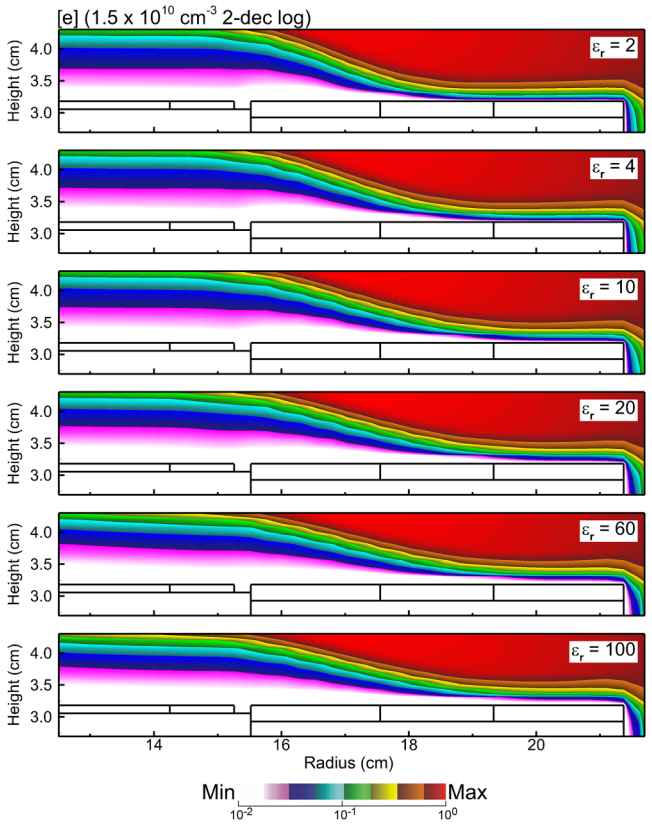

FIG. 4. Time averaged electron densities above the edge of the wafer and FR for subsurface FR dielectric constants ε_r ranging from 2 to 100. The other conditions are the same as for the base case. With increasing ε_r, the sheath potential and thickness above the FR increases.

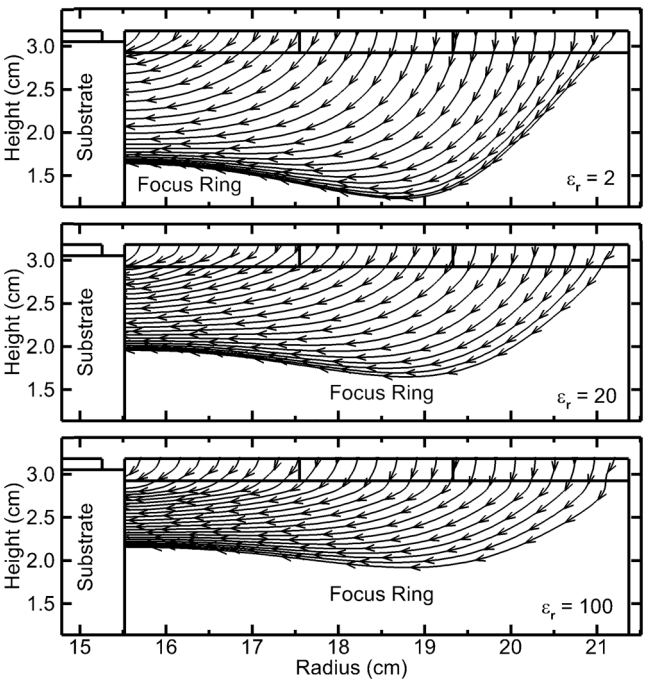

FIG. 5. Electric field streamlines originating at the top of the FR and terminating on the powered substrate. The streamlines are averaged over the low frequency RF cycle for (top) $\varepsilon_r = 2$, (middle) $\varepsilon_r = 20$, and (bottom) $\varepsilon_r = 100$.

wafer and FR are nearly insensitive to the value of ε_r, differing by only few to 10%. The ion fluxes to the wafer are also not particularly sensitive functions of ε_r. Since the power deposition is constant and the permittivity of the focus ring dominantly affects sheath properties, to which ions are more sensitive, the generation of reactive species is not greatly changed for moderate changes in ε_r. It is only at larger values of ε_r that reactive fluxes begin to change—a decrease above the wafer and an increase above the FR. With increasing ε_r, more current flows through the FR compared to the wafer, enabling more power deposition above the FR, which, for constant power deposition, is at the expense of power deposition over the wafer.

With a larger ε_r, the impedance of the FR decreases and the division of voltage between the FR and the sheath above the FR begins to favor the sheath. With an increase of ε_r, less voltage is dropped across the focus ring and more voltage is dropped across the sheath. The end result is a thickening of the sheath with increasing ε_r and an improvement in the uniformity of the sheath across the FR, as shown in Fig. 4.

A direct consequence of the shifting of voltage from the FR to sheath above the FR when increasing ε_r is an extension in energy and narrowing in angle of the IEADs incident onto the FR. This trend applies to all locations but is most prominent at locations D and E, the center and outer edge of the FR. The IEADs incident onto the middle (location A) and edge of the wafer (B) are shown in Fig. 7 for $\varepsilon_r = 2$, 4, 10, 20, 60, and 100. The IEADs incident onto the inner edge (location C), middle (D), and outer edge (E) of the FR are shown in Fig. 8. The IEADs over the wafer are nearly independent of permittivity of the FR up until $\varepsilon_r = 20$. Above this permittivity, the power dissipated above the FR becomes a significant fraction of the total power. This redistribution of power effectively increases the surface area of the powered electrode, which then enables a lower voltage amplitude for constant total power deposition. The DC bias then also decreases in magnitude (less negative). To deliver 1000 W at 5 MHz, the voltage amplitude decreases from 1650 V (DC bias −1200 V) for $\varepsilon_r = 2$ to 1265 V (DC bias −925 V) at $\varepsilon_r = 100$. With this decrease in voltage amplitude and DC bias with increasing ε_r, the maximum energy of the IEADs onto the wafer decreases (locations A and B).

The trends in IEADs above the FR have the opposite trend with increasing ε_r compared to IEADs over the wafer, as shown in Fig. 8. At the center (location D) and outer edge (E) of the FR, the IEADs onto the surface increase in maximum energy and become narrow in angular spread as ε_r increases. At the center of the FR (D), the maximum energy increases from 180 eV for $\varepsilon_r = 2$ to 400 eV for $\varepsilon_r = 100$. For the right edge of the FR (E), the increase in maximum energy is from 35 to 110 eV. This increase in energy,

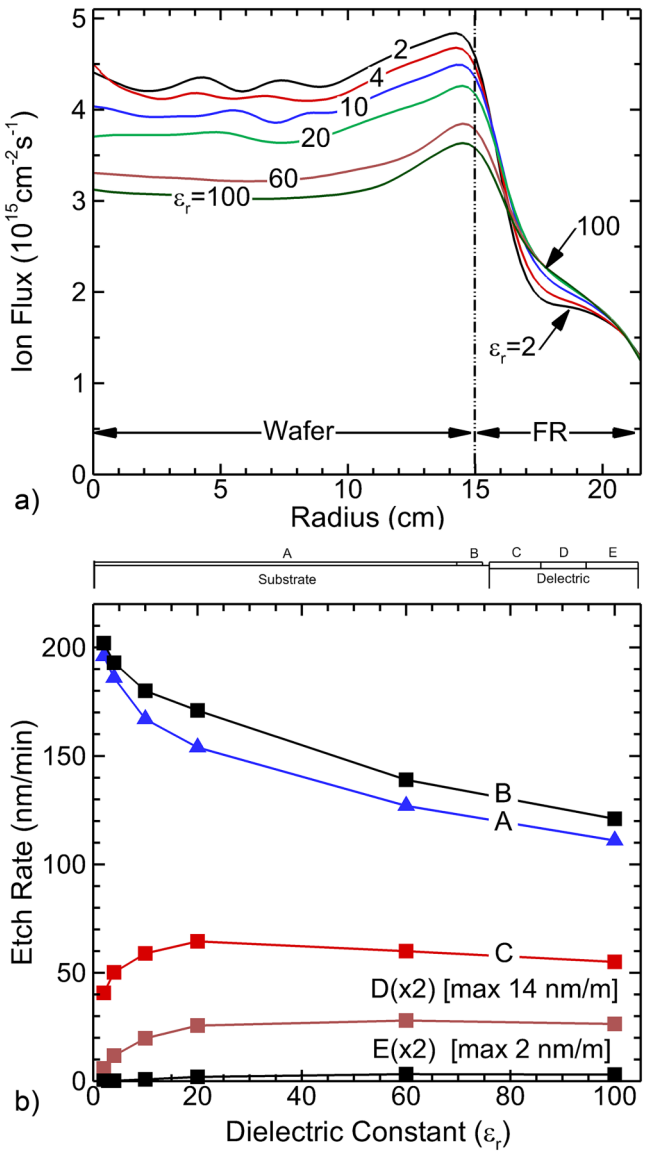

FIG. 6. Plasma properties and etch rates as a function of the sub-FR dielectric constants ε_r ranging from 2 to 100 for otherwise the base case conditions (Ar/C_4F_8/O_2 = 75/20/5, 600 SCCM, 30 mTorr, 60/5 MHz = 600/1000 W). (a) Time averaged total ion flux to the wafer and FR. (b) SiO_2 etch rate at locations A–E, identified in the schematic. Note that etch rates for locations D and E are multiplied by a factor of 2 for clarity. The other conditions are the same as the base case.

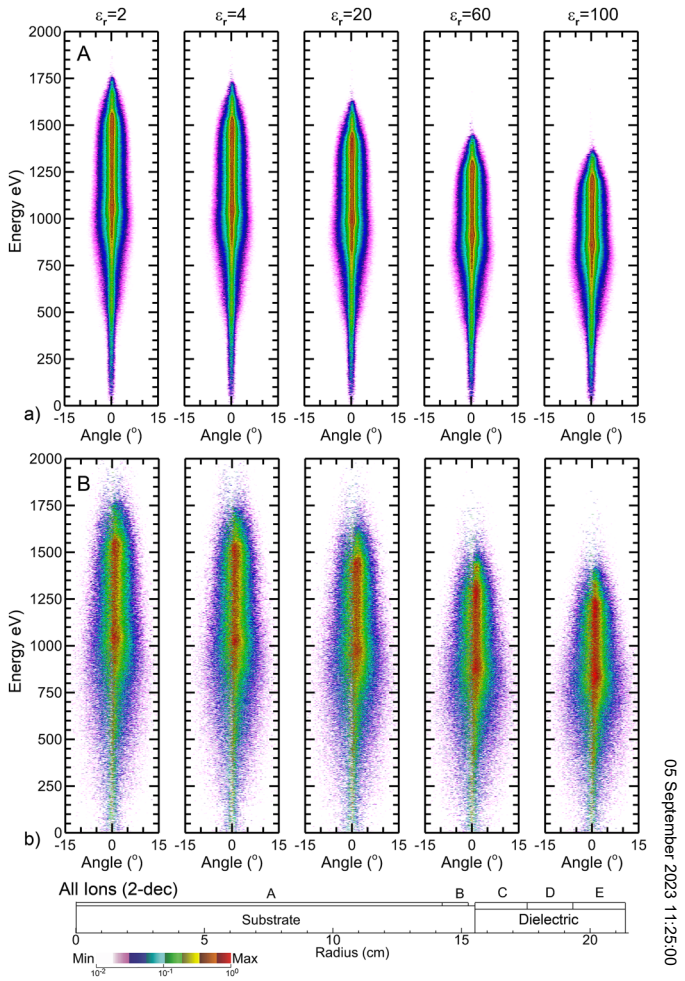

FIG. 7. Ion energy and angular distributions for values of the subsurface FR dielectric constants ε_r ranging from 2 to 100 at wafer locations (a) A and (b) B, indicated in the bottom schematic. Each IEAD is separately normalized and plotted on a two-decade log scale. With increasing ε_r, the maximum energy of the IEAD over the wafer decreases.

beginning at about $\varepsilon_r = 20$, is a direct consequence of the increase in capacitance of the FR compared to the sheath above the focus ring. The resulting voltage division then favors the sheath which, on a relative basis, has a larger impedance. The increase in the relative impedance of the sheath above the FR results in establishing an RF cycle-averaged sheath (see Fig. 4) that is thicker and has a larger sheath potential that accelerates ions into the FR. At the pressures of interest (30 mTorr here), the sheath is largely collisionless, and so thickening of the sheath above the FR is not a detriment to the maximum ion energy.

The increase in the energy of the IEAD in the center of the FR (location D) occurs at a lower ε_r than at the outer edge (location E). The angular distribution at the center of the FR is also asymmetric at the highest energies at all values of ε_r. These trends are explained by the shape of the sheath, as shown in Fig. 4. As the sheath thickness, λ, transitions from being thicker over the wafer ($\lambda \approx 2750\,\mu$m) to being thinner over the FR ($\lambda < 750\,\mu$m), there is a slope to the edge of the sheath. This slope begins at the edge of the wafer and extends to approximately the middle of the FR. The change in thickness of the sheath is largely a consequence of the

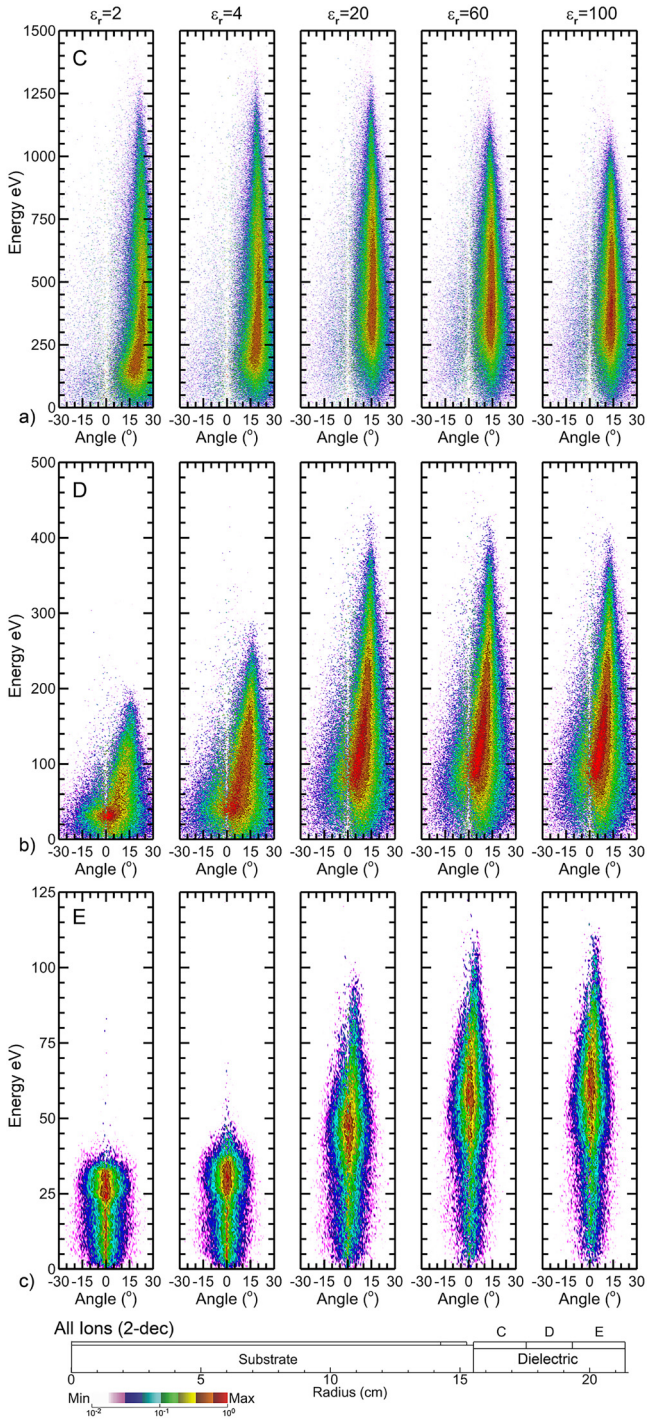

FIG. 8. IEADs for values of the sub-FR dielectric constants ε_r ranging from 2 to 100 at FR locations (a) C, (b) D, and (c) E, indicated in the bottom schematic. Each IEAD is separately normalized and plotted on a two-decade log scale. With increasing ε_r, the maximum energy of the IEAD over the FR increases with a larger angular skew.

reduction in sheath potential from the wafer to the FR. However, there is also a component of the capacitance of the FR at the plasma facing surface, C_{FR} (F/cm^2), being a function of position. The capacitance at the surface of the focus ring is dependent on the path of the electric field line that begins at the surface of the biased substrate and terminates at the surface of the FR—the shorter the path length the larger the capacitance. With the path length from the powered substrate to the sites on the FR smaller radii being shorter than sites having larger radii, C_{FR} is larger at smaller radii. The larger C_{FR} then favors the sheath above the FR in voltage division. As ε_r increases and the sheath thickens above the FR, the slope of the sheath lessens, which results in a more angularly symmetric IEAD.

The IEAD onto the edge of the FR is most angularly asymmetric at the highest energies. This results from the sheath being thickest over the wafer, while being thin across the FR, when the sheath potential over the wafer has its largest value. This occurs when the voltage on the substrate is most negative. The sheath is least angled over the edge of the FR when the sheath potential collapses during the anodic portion of the cycle, being thin across both the wafer and the FR. These trends produce the most angularly symmetric ion fluxes at low energy and the most angularly skewed ion fluxes at high energy. With the slope in the sheath being most severe at low ε_r, the angular skew in the IEAD at the edge of the wafer (location B) is also most severe with low ε_r. For example, for $\varepsilon_r = 2$, the skew in the IEAD at high energy is 2°, while at $\varepsilon_r = 100$, the skew is 0.6°.

The IEAD at the inner edge of the FR (location C) is something of a compromise or average of the trends over the wafer and over the FR. The maximum energies of IEADs over the wafer generally decrease with increasing ε_r while the maximum energies of IEADs over the FR increase with increasing ε_r. These opposing trends result in the IEAD at the edge of the FR having a maximum energy (1250 eV) that is intermediate between wafer and FR, with the maximum energy occurring at $\varepsilon_r \approx 20$. With the edge of the FR always being in the transition between the thick sheath over the wafer and thinner sheath over the FR, the angular distributions are asymmetric at all values of ε_r. The largest asymmetry occurs for $\varepsilon_r \approx 20$ where there is the largest difference in thickness of the sheath from over the wafer to over the FR.

Etch rates for SiO_2 across the wafer and FR as a function of ε_r are shown in Fig. 6(b). ERs over the wafer are above 100 nm/m for all values of ε_r. With the IEADS at the center (location A) and edge (location B) of the wafer being nearly the same, the larger value of ER at the edge of the wafer is attributed to the larger ion flux [shown in Fig. 6(a)]. The general trend of decreasing ER over the wafer with increasing ε_r results in part from the decrease in the maximum energy of the IEADs (Fig. 7) and results in part to the decrease in ion flux [Fig. 6(a)].

The etch rates across the FR have the opposite trend with increasing ε_r as those over the wafer. Over the FR, the ER increases with increasing ε_r. This increase in ER is partly due to the increase in ion flux with increasing ε_r, though the increase in ion flux can account for only about 10%–20% of the increase in ER. The majority of the increase in ER results from the increase in maximum energy of the IEADs with increasing ε_r. With the increase in maximum energy of the IEAD over the FR occurring at smaller ε_r for smaller

radii, the ER also increases more rapidly with ε_r at smaller radii. Again, the ER at the inner edge of the FR (location C) is a compromise between the trends for the wafer and FR. The ER at the inner edge of the FR has a maximum at $\varepsilon_r = 20$, which corresponds to the value of ε_r at which the IEAD reaches its maximum energy.

As mentioned in the Introduction, the FR in most plasma etching tools used in HVM is a consumable part. There is great motivation to minimize the erosion of the FR to both maintain a consistent process and to minimize the cost and frequency of replacing the FR. These results indicate that using a focus ring with a small ε_r will minimize etch rates and lengthen the lifetime of the FR. The trade-off is that with smaller ε_r the slope of the sheath at the edge of the wafer is most severe and the angular skew of the IEAD at high energies is largest. For example, for the particular reactor configuration used in this study, the angular skew of the IEAD averaged over the wafer (excluding the edge region B) is less than 0.25° and is independent of ε_r. (These angular skews are averaged over all ions and energies.) At the edge of the wafer (location B), the average angular skew is a minimum of 0.4°–0.5° for $\varepsilon_r = 100$ and a maximum of 1.0°–1.1° for $\varepsilon_r = 20$. For systems that have a smaller gap between the wafer and the FR than used here, the more severe slope of the sheath could lead to a more severe angular skew at the edge of the wafer at low values of ε_r, with the most severe skew occurring for the highest ion energies for which the etch rates are the largest. These non-normal angular distributions can produce tilting or twisting to HAR features.[20] One potential remedy would be to grade the permittivity of the FR to minimize angular skew and erosion. These results suggest that having a high value of ε_r at the inner edge of the FR and low value at the out edge of the FR might provide this trade-off. This could be accomplished by having discrete annuli of subsurface materials having graded dielectric constant—high at smaller radius and low at larger radius.

There are other considerations in HVM in choosing the material and physical properties of the FR. Regardless of the etch rate of the top layer of the FR, thinner layers will need to be replaced more frequently as part of preventative maintenance (PM). This higher rate of replacement becomes expensive and increases the frequency of PM. A thicker layer may increase the time between PM but may not optimize etch properties.

In principle, the materials used for the sub-FR to control the permittivity can be isolated from the plasma by using chemically compatible barrier coatings on the surface of the FR (other than the top). Since these coatings will be thin and their capacitances large, the coatings will make a small contribution to the total impedance. Assuming use of such a barrier coating, the material of the sub-FR does not need to be chemically compatible with the process. The material could, in principle, be simply vacuum (gas) that would provide the minimum ε_r. At the other extreme, materials such as titanates could

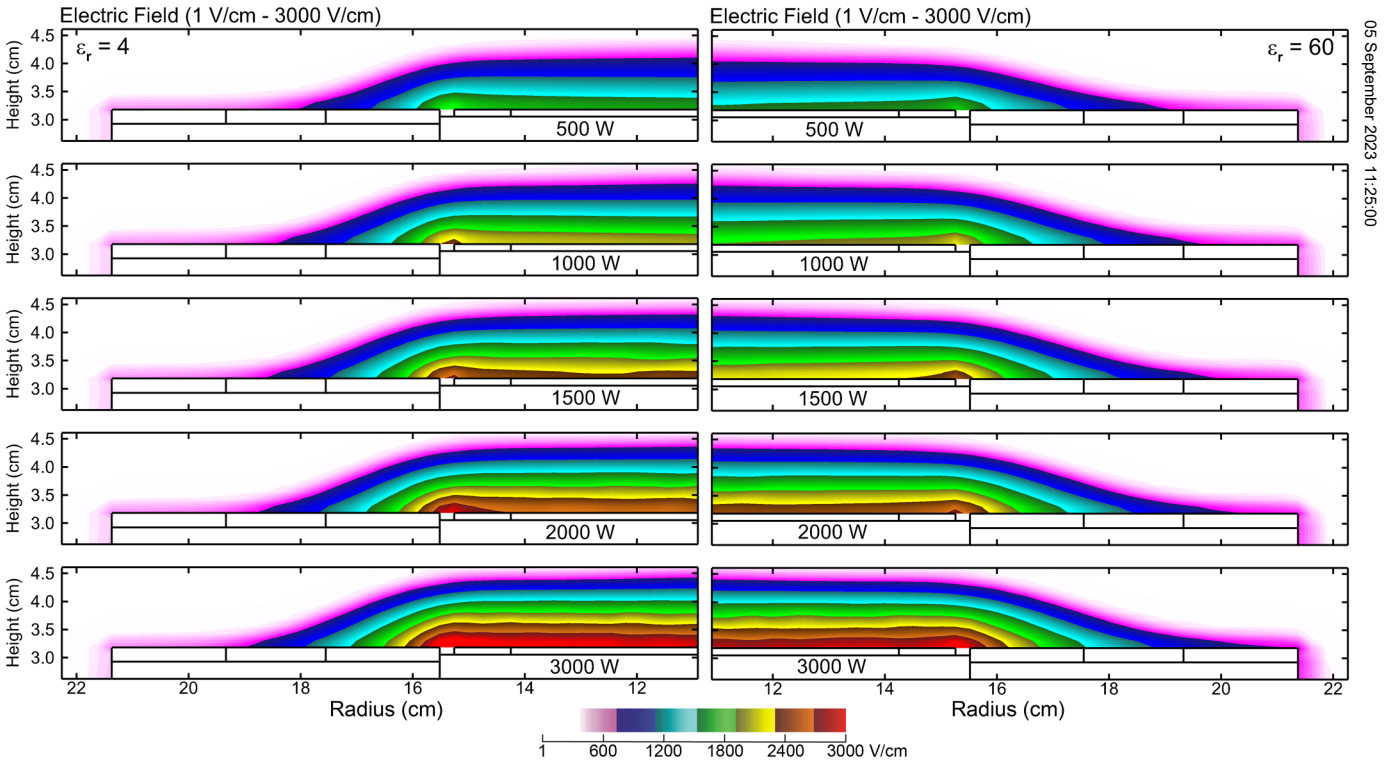

FIG. 9. Time averaged electric field above the outer radius of the wafer and FR for low frequency powers of (top to bottom) 500–3000 W, and for FR dielectric constants of (left) $\varepsilon_r = 4$ and (right) $\varepsilon_r = 60$.

be used which have ε_r values of hundreds. For example, dielectric constants of polymer-titanate composites can be continuously varied up to 130 with nearly flat frequency response up to 10^7 Hz.[21]

V. FR EROSION VS LOW FREQUENCY BIAS POWER

When plasma etching HAR features, IEADs with high energy and narrow angular distributions are desired. In multifrequency CCPs, these properties are usually obtained by increasing power of the lowest RF bias frequency on the substrate. IEADs and FR erosion were investigated as a function of the LF power. Cycle-averaged electric fields for LF powers of 500–3000 W are shown in Fig. 9 over the outer few centimeters of the wafer and over the FR for $\varepsilon_r = 4$ and 60. The IEADs for these conditions at the center of the FR (location D) are shown in Fig. 10. The conditions are otherwise the same as the base case with the power of the high frequency remaining constant at 600 W. The intent of the LF is to accelerate ions into the substrate without affecting plasma properties, which should, ideally, be controlled by the HF power. However, with LF power extending to five times that of the HF power, there is some inevitable additional plasma production. For example, for $\varepsilon_r = 4$, the electron density at midgap (radius = 10 cm) increases from 1.2×10^{10} cm^{-3} for an LF power of 500 W to 2.5×10^{10} cm^{-3} for an LF power of 3000 W. For $\varepsilon_r = 60$, the increase is 1.2×10^{10} cm^{-3} for an LF power of 500 W to 2.4×10^{10} cm^{-3} for an LF power of 3000 W.

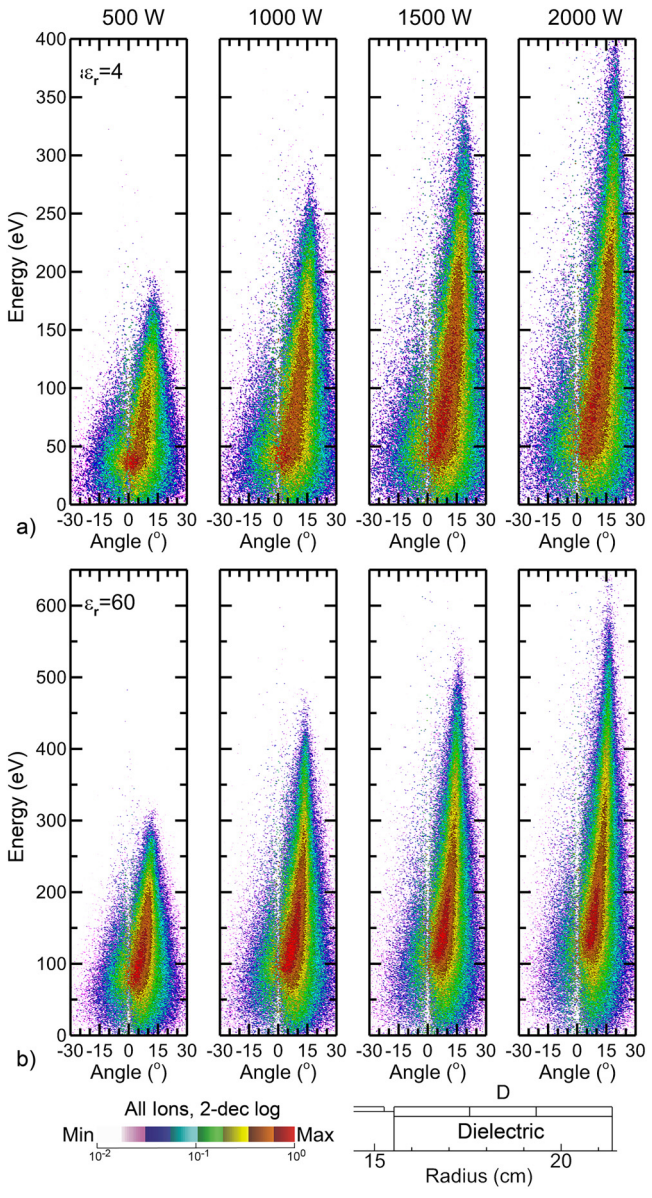

FIG. 10. IEADs at location D on the FR for low frequency powers of 500–2000 W. IEADs are shown for subsurface FR dielectric constants of (a) $\varepsilon_r = 4$ and (b) $\varepsilon_r = 60$. Each IEAD is separately normalized and plotted on a two-decade log scale. With increasing power, the angular skew of the IEAD also increases.

With $\varepsilon_r = 4$, the capacitance of the FR is small compared to that of the sheath. As a result, regardless of the LF power, the majority of the bias voltage is dropped across the FR, and the sheath thickness above the FR, as shown in Fig. 9, does not significantly increase with increasing LF power. The sheath also does not significantly extend to larger radius on the FR. In contrast, the sheath above the wafer thickens above the wafer with increasing LF power, reflecting the increase in voltage amplitude and magnitude of the DC bias (more negative). For $\varepsilon_r = 4$, the 5 MHz voltage amplitude is 1140 V (DC bias −865 V) for an LF power of 500 W and 2725 V (DC bias −1970V) for 3000 W. For $\varepsilon_r = 60$, the 5 MHz voltage amplitude is 1030 V (DC bias −765 V) for an LF power of 500 W and 2565 V (DC bias −1830 V) for 3000 W. As a result, the slope of the sheath at the edge of the wafer becomes more severe with the increase in power, which also extends the high potential sheath over the FR.

The IEADs to the center of the FR (location D) reflect these trends, as shown in Fig. 10. For $\varepsilon_r = 4$, the maximum energy of the IEAD increases from 175 to 400 eV for LF powers of 500–3000 W, while for $\varepsilon_r = 60$, the increase is 300–575 eV. The IEAD consists of low energy and high energy components. For $\varepsilon_r = 4$, the low energy component is nearly angularly symmetric for an LF power of 500 W while its high energy component has an angular skew of 11°. For an LF power of 3000 W, the skew is 7° for the low energy component and 18° for the high energy component. The angular skews are similar for $\varepsilon_r = 60$.

ERs as a function of position on the wafer (locations A–E) for LF powers of 500–3000 W are shown in Fig. 11 for $\varepsilon_r = 4$ and 60. Over the wafer, the etch rates scale approximately with LF power. (The edge-high etch rate results from the particular geometry used for this study.) The same general scaling in ER applies to the inner edge and middle of the FR. For $\varepsilon_r = 4$, etch rates at the middle of the FR (location D) increase from 3.3 to 19 nm/m for 500–3000 W. At the outer edge of the FR (location E), the increase is from 0.1 to 0.8 nm/m. The ER is small at the outer edge of the FR due to the majority of the IEAD being below threshold for chemical sputtering. For $\varepsilon_r = 60$, etch rates at the middle of the FR increase from 8.7 to 35 nm/m for 500–3000 W. The increase in etch rate with increasing LF power is of about a factor of 2–2.5 larger compared to $\varepsilon_r = 4$ due

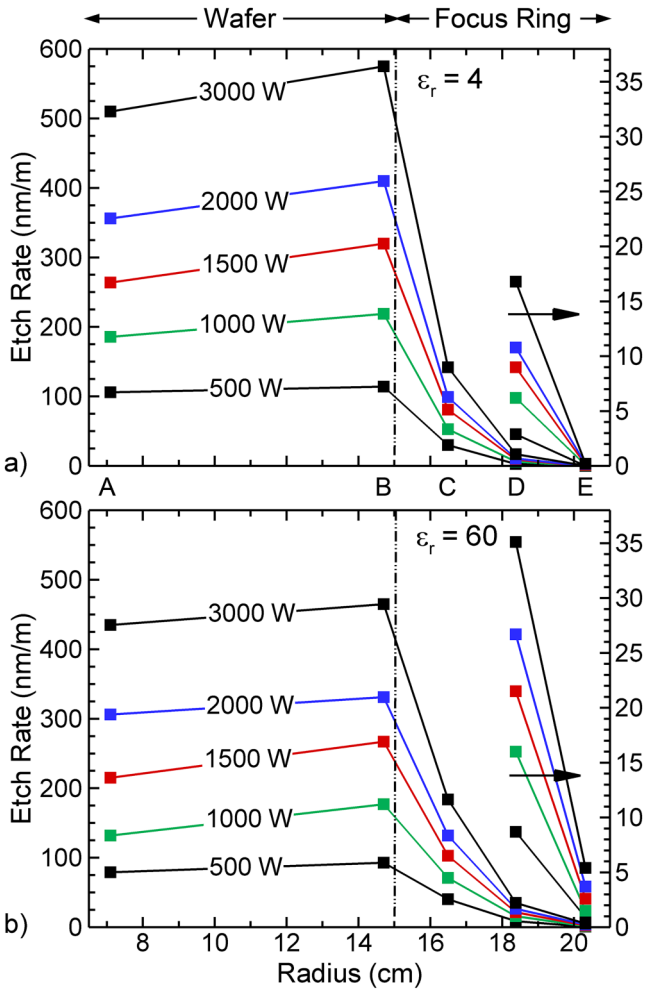

FIG. 11. SiO_2 etch rates over the wafer and FR for low frequency powers of 500–3000 W. Etch rates are shown for subsurface FR dielectric constants of (a) $\varepsilon_r = 4$ and (b) $\varepsilon_r = 60$. The etch rates on the FR are also shown on an expanded scale on the right vertical axis.

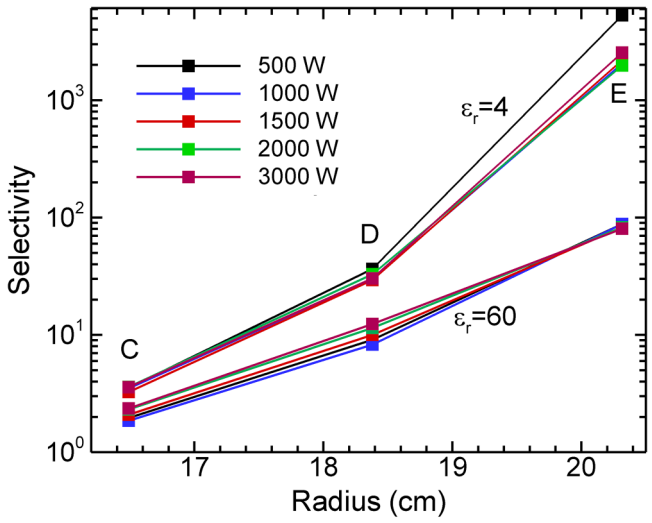

FIG. 12. Etch selectivity [defined as (etch rate of wafer)/(etch rate of FR)] at locations C, D, and E on the FR. for low frequency powers of 500–3000 W. Selectivity is shown for subsurface FR dielectric constants of $\varepsilon_r = 4$ and $\varepsilon_r = 60$.

to the greater increase in ion energies. At the outer edge of the FR, the increase in ER for $\varepsilon_r = 60$ is from 1 to 6 nm/m. These values are 8–10 times those for $\varepsilon_r = 4$ as a result of the ion energies for $\varepsilon_r = 60$ increasing above the chemical sputtering threshold.

From the perspective of HVM, the important parameter is selectivity of etching of the wafer compared to the FR. Selectivity is the etch rate of the wafer divided by the etch rate of the FR. To have a long lifetime of the FR (long time between replacement), selectivity should be large and ideally would be infinite—no etching of the FR. The selectivity of etching across the FR for LF powers of 500–3000 W for $\varepsilon_r = 4$ and $\varepsilon_r = 60$ is shown in Fig. 12. Predicted selectivities are as low as 2 (inner edge of FR, high ε_r) to as high as 5000 (outer edge of FR, low ε_r). The general trend is higher selectivity for lower ε_r as ion energies onto the FR are generally lower for low ε_r. Selectivity increases from the inner edge to outer edge of FR, which reflects the decrease in ion energy. Surprisingly, selectivity is not a strong function of LF power for a given location and ε_r. The relative increase in etch rate with power is nearly the same on the wafer and FR. The exception is at the outer edge of FR for high ε_r where high powers produce lower selectivity as ion energies broach the chemical sputtering threshold.

VI. CONCLUDING REMARKS

The erosion of FR in a dual-frequency CCP reactor sustained in an $Ar/C_4F_8/O_2$ mixture was investigated for SiO_2 blanket etching while varying the dielectric constant (ε_r) of the FR and the LF power. With increasing ε_r of the FR, ion energies incident onto the wafer generally decreased and those incident onto the FR increased. These trends result from the capacitance of the FR increasing (and impedance decreasing) relative to the sheath above the FR. The end result is that more voltage dropped across the sheath above the FR, producing more energetic ions onto the FR. With more power dissipated above the FR and a more symmetric distribution of power in the reactor, the voltage amplitude and magnitude of the DC bias decrease with increasing ε_r, which reduces ion energies onto the wafer. The angular distributions of ions onto the FR are skewed from the normal, a consequence of the slope of the sheath transitioning from being thick over the wafer to thin over the FR. This skew can extend to the edge of the wafer.

Selectivity of etching the wafer compared to the FR is an important parameter in determining the lifetime of the FR. Selectivity generally decreases as ε_r increases in response to the increase in ion energies onto the FR. A portion of this increase (10%–20%) results from an increase in ion flux onto the FR. There is a significant increase in selectivity from the inner to outer edge

of the FR, a consequence of the ion energies onto the FR being largely below the chemical sputtering threshold.

The purpose of the FR is to extend the uniformity of reactant fluxes to the edge of the wafer and so minimize the edge-exclusion while minimizing the erosion of the FR. The choice of materials of plasma facing surface of the FR is predicated, in part, on the need for chemical compatibility with the wafer. There may be limited options to meet this need. However, the subsurface materials of the FR, which are not exposed to the plasma, do not have this limitation. For these materials, electrical properties such as dielectric constant can be chosen to optimize the transition in reactant fluxes in crossing from the wafer to the FR. Here, one might consider grading the electrical properties of the FR as a function or radius to minimize skewing of the IEAD at the edge of the wafer while minimizing erosion of the FR.

Another design trade-off is the thickness of the top surface of the FR. The capacitance of the focus ring consists of the series capacitance of the top layer and subsurface portions. In principle, the top layer can be made arbitrarily thin (large capacitance) so that the electrical properties of the FR are dominantly determined by the subsurface material. However, a thinner top layer while having a finite rate of erosion will require more frequent replacement.

ACKNOWLEDGMENTS

This work was supported by Samsung Electronics Ltd. and the National Science Foundation (No. PHY-2009219). These results were also based on work supported by the U.S. Department of Energy, Office of Science, Office of Fusion Energy Sciences, under Award No. DE-SC0020232.

DATA AVAILABILITY

The data that support the findings of this study are available from the corresponding author upon reasonable request.

REFERENCES

[1]C. G. N. Lee, K. J. Kanarik, and R. A. Gottscho, J. Phys. D: Appl. Phys. **47**, 273001 (2014).
[2]D. Kim and D. J. Economou, J. Appl. Phys. **95**, 3311 (2004).
[3]H. J. Kim and H. J. Lee, Plasma Sources Sci. Technol. **25**, 065006 (2016).
[4]L. Tong, Jpn. J. Appl. Phys. **54**, 06GA01 (2015).
[5]Y. Cui *et al.*, J. Micromech. Microeng. **29**, 105010 (2019).
[6]K. C. Yang, S. W. Park, H. S. Lee, D. W. Kim, and G. Y. Yeom, Nanosci. Nanotechnol. Lett. **9**, 24 (2017).
[7]A. Suzuki, N. Terasawa, T. Moriya, and S. Y. Kang, *International Symposium on Semiconductor Manufacturing (ISSM 2010)*, Tokyo, Japan (IEEE, Tokyo, 2010), paper PO-O-098m.
[8]T. Yamaguchi *et al.*, Jpn. J. Appl. Phys. **50**, 056101 (2011).
[9]I.-Y. Jang, J.-Y. Lee, Y-H. Kim, S.-W. Choi, and J.-M. Sohn, Proc. SPIE **5130**, 246 (2003).
[10]J. S. Kim, M. Y. Hur, H. J. Kim, and H. J. Lee, J. Appl. Phys. **126**, 233301 (2019).
[11]N. Y. Babaeva and M. J. Kushner, J. Appl. Phys. **101**, 113307 (2007).
[12]K. Denpoh and T. Shirafuji, Jpn. J. Appl. Phys. **49**, 056202 (2010).
[13]N. Y. Babaeva and M. J. Kushner, J. Phys. D: Appl. Phys. **41**, 062004 (2008).
[14]M. J. Kushner, J. Phys. D: Appl. Phys. **42**, 194013 (2009).
[15]A. V. Vasenkov, X. Li, G. S. Oehrlein, and M. J. Kushner, J. Vac. Sci. Technol. A **22**, 511 (2004).
[16]A. V. Vasenkov and M. J. Kushner, J. Appl. Phys. **95**, 834 (2004).
[17]S. Huang, C. Huard, S. Shim, S. K. Nam, I.-C. Song, S. Lu, and M. J. Kushner, J. Vac. Sci. Technol. A **37**, 031304 (2019).
[18]B. S. Kwon, J. S. Kim, N.-E. Lee, and J. W. Shon, J. Electrochem. Soc. **157**, D135 (2010).
[19]S. Rauf and A. Balakrishna, J. Vac. Sci. Technol. A **35**, 021308 (2017).
[20]N. Negishi, M. Miyake, K. Yokogawa, M. Oyama, T. Kanekiyo, M. Izawa, J. Vac. Sci. Technol. B **35**, 051205 (2017).
[21]L. Dong, C. Xiong, H. Quan, and G. Zhao, Scr. Mater. **55**, 835 (2006).